



## PELDOR on an exchange coupled nitroxide copper(II) spin pair

Bela E. Bode<sup>a</sup>, Jörn Plackmeyer<sup>a</sup>, Michael Bolte<sup>b</sup>, Thomas F. Prisner<sup>a</sup>, Olav Schiemann<sup>a,1,\*</sup>

<sup>a</sup>Institute of Physical and Theoretical Chemistry and Center for Biomolecular Magnetic Resonance, Goethe University, Max-von-Laue-Strasse 7, 60438 Frankfurt am Main, Germany

<sup>b</sup>Institute of Inorganic and Analytical Chemistry, Goethe University, Max-von-Laue-Strasse 7, 60438 Frankfurt am Main, Germany

### ARTICLE INFO

#### Article history:

Received 31 July 2008

Received in revised form 20 October 2008

Accepted 14 November 2008

Available online 24 November 2008

Dedicated to Prof. Ch. Elschenbroich on the occasion of his 70th birthday.

#### Keywords:

EPR

DEER

Exchange coupling

Dipolar coupling

Porphyrin

Metal ions

### ABSTRACT

Transition metal ions play an important role in the design of macromolecular architectures as well as for the structure and function of proteins and oligonucleotides, which makes them interesting targets for spectroscopic investigations. In combination with site directed spin labelling, pulsed electron–electron double resonance (PELDOR or DEER) could be a well-suited method for their characterization and localization. Here, we report on the synthesis and full characterization of a copper(II) porphyrin/nitroxide model system bearing an extended  $\pi$ -conjugation between the spin centres and demonstrate the possibility to disentangle the dipolar through space interaction from the through bond exchange coupling contribution even in the presence of orientational selectivity and conformational flexibility. The simulations used are based on the known experimental and spin Hamiltonian parameters and on a structural model as previously employed for similar systems. The mean exchange coupling of +4(1) MHz (antiferromagnetic) is in agreement with the value of  $|J| = 3(1)$  MHz determined from room temperature continuous wave electron paramagnetic resonance (EPR). Thus, as long as the pulse excitation bandwidths are large versus the spin–spin coupling, X-band PELDOR measurements in combination with explicit time trace simulations allow for disentangling the sign and magnitude of through bond electron–electron exchange from the through space dipolar interaction  $D$ .

© 2008 Elsevier B.V. All rights reserved.

### 1. Introduction

Transition metal ions play an important role in the design of macromolecular architectures [1] as well as the structure and function of proteins [2] and oligonucleotides [3]. Structures of such assemblies, and therefore a key to their function, can be obtained via X-ray diffraction or NMR spectroscopy. However, the former method fails if the sample is non-crystalline and the latter reaches its limits if the metal ions are paramagnetic and/or the assembly becomes too large. On the other hand modern pulsed EPR methods have shown to yield not only precise electronic and geometric information about metal ion binding pockets [4] but also to reveal long-range arrangements on the nanometre scale via the dipolar coupling between paramagnetic centres [5]. One of the latter methods is called pulsed electron–electron double resonance (PELDOR or DEER) [6], which has been shown to very reliably measure distances of up to 6 nm between two organic radicals [7] including distance distributions [8], angular information [9] and the number of coupled spins [10]. Over the last years, this method has been extended to paramagnetic metal centres involving copper(II)/nitroxide [11] copper(II)/copper(II) [12], and gadolinium(III)/gadol-

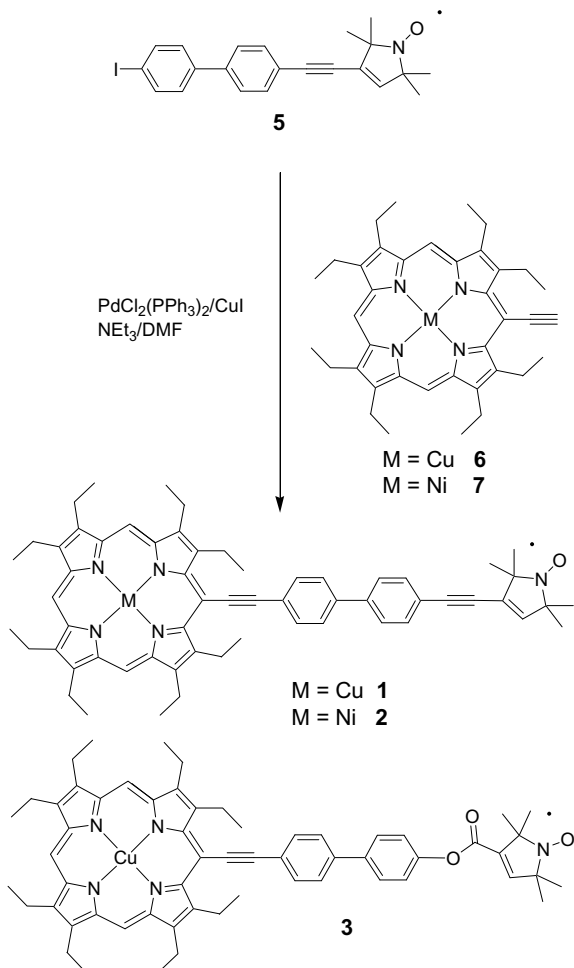
linium(III) pairs [13], as well as distances between iron–sulphur clusters and a nickel–iron centre [14] or an organic radical [15]. Such systems are more demanding, due to several reasons. First, they usually have a large hyperfine- and  $g$ -tensor anisotropy, which results in broad EPR spectra from which the pulses excite only a fraction which can induce a strong orientation selection. Second, the relaxation time might be fast, which narrows the detection window and limits thereby the accessible distance range. And third, the spin density might be distributed into the ligands, leading to the breakdown of the simple point–dipole model and the onset of an exchange coupling  $J$ .

Since copper(II) centres often occur in biological systems and are frequently used for building supramolecular assemblies a deeper and quantitative understanding of PELDOR spectra from such centres is needed. We therefore synthesized model system **1** in which a copper(II)porphyrin is connected via a conjugated bridge to a nitroxide as well as the reference molecule **2** in which the paramagnetic copper(II) is exchanged for the diamagnetic nickel(II) ion (Scheme 1). Recently, we have shown for a similar model system **3** [16] (Scheme 1), in which the conjugation of the bridge is disrupted by an ester linkage, that the broad copper spectrum induces orientation selection, but that its effect on the PELDOR spectra is weak. It could also be demonstrated that the point–dipole model is still valid despite the considerable delocalization of spin density from the copper into the porphyrin ring. The reason for the former is the large hyperfine coupling of the ring nitrogens,

\* Corresponding author. Tel./fax: +44 1334 46 3410.

E-mail address: [os11@st-andrews.ac.uk](mailto:os11@st-andrews.ac.uk) (O. Schiemann).

<sup>1</sup> Present address: Centre for Biomolecular Sciences, Centre of Magnetic Resonance, University of St. Andrews, St. Andrews, Fife, KY16 9UA Scotland, United Kingdom.



**Scheme 1.** Synthesis of model compounds **1** and **2**. For the sake of comparison, the scheme also shows reference molecule **3**, previously reported.

leading to orientational “smearing”. The reason for the latter is the concentric distribution of spin density resulting only in a small orthorhombic contribution to the dipolar tensor [17].

Here, we were interested whether the conjugated bridge in **1** would go in-parallel with an increase in the exchange coupling constant  $J$  compared to **3**, which displayed a distribution in  $J$  of  $\Delta J = \pm 1$  MHz centred around  $J = 0$  MHz; and if so, how it effects would be on the PELDOR time traces and whether it would be possible to disentangle the dipolar through space interaction  $D$  from the through bond exchange coupling contribution  $J$ . Especially, the last point is of concern, because if this is not possible the error in mean distances and distance distributions will dramatically increase.

### 1.1. PELDOR theory

All following PELDOR experiments were performed with the 4-pulse sequence shown in Fig. 1.

The pulses at the detection frequency  $\nu_A$  create an echo from the spins on resonance, named in the following A spins (the unpaired electron centred at the Cu(II)porphyrin in this study). Introduction of an inversion pulse at the pump frequency  $\nu_B$  flips spins resonant with this second frequency, here defined as B spins (here the electron spin centred at the nitroxide). The coupling  $\omega_{AB}$  between the A and B spins causes a shift in the Larmor frequency of the A spins by  $\pm\omega_{AB}$ . Therefore, after pumping the B spins the A spins accumulate a phase shift  $\omega_{AB}t$ , where  $t$  defines the time delay of the pump

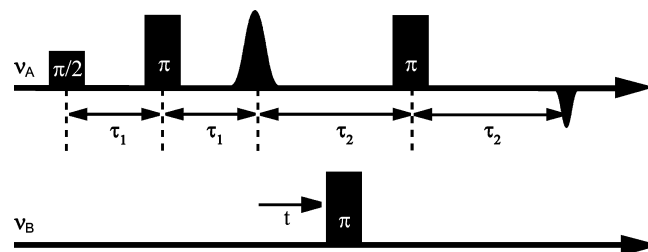


**Fig. 1.** Pulse sequences for 4-pulse PELDOR.

pulse. The resulting PELDOR signal  $V(t)$  is a product of two contributions

$$V(t) = V_{\text{intra}}(t)V_{\text{inter}}(t). \quad (1)$$

$V_{\text{intra}}(t)$  describes the intramolecular contribution, whereas  $V_{\text{inter}}(t)$  takes into account the signal decay with  $t$  caused by intermolecular interactions. In case of a homogeneous distribution of the molecules  $V_{\text{inter}}(t)$  is a monoexponential decay [18]. In the general case of disordered samples and angular correlations between the spin centres, the echo signal intensity of the intramolecular contribution  $V_{\text{intra}}(t)$  is given by [19].

$$V_{\text{intra}}(t) = V_0 \left( 1 - \left[ \int_0^{\pi/2} P(\theta) [1 - \cos(\omega_{AB}t)] d\theta \right] \right) \quad (2)$$

with

$$P(\theta) = \lambda(\theta) \sin \theta. \quad (3)$$

$V_0$  is the spin echo intensity at  $t = 0$ , given by the fraction of spins A excited by the detection pulses.  $P(\theta)$  is the distribution function of dipolar angles  $\theta$  excited by the pulse sequence. It takes into account the orientation selection of the detection pulses and of the pump pulse and includes the dependence of the excitation efficiency  $\lambda(\theta)$  of the pump pulse on the mutual orientation of the two radicals A and B.  $\sin(\theta)$  is the distribution function of uncorrelated radical pairs. In the point-dipole approximation and for small  $g$ -anisotropies, such that the spin states are quantized parallel to the external field, and in the weak coupling regime, the coupling  $\omega_{AB}$  between the two spins is described by the sum of the dipolar contribution  $\omega_{DD}$  mediated through space and the exchange coupling constant  $J$  mediated through bond.

$$\omega_{AB} = \omega_{DD} + J. \quad (4)$$

The dipolar contribution is expressed by Eq. (5) and  $J$  is defined via the spin Hamiltonian  $H = JS_{zA}S_{zB}$ .

$$\omega_{DD} = -\frac{\mu_0 \mu_B^2}{4\pi \hbar} \frac{g_A g_B}{|r_{AB}|^3} (3 \cos^2 \theta - 1). \quad (5)$$

In Eq. (5),  $g_A$  and  $g_B$  are the  $g$ -values of the spins A and B, respectively,  $\hbar$  is the Planck constant divided by  $2\pi$ ,  $r_{AB}$  is the distance vector connecting the spins,  $\theta$  is the angle between  $r_{AB}$  and the external magnetic field, and  $\mu_0$  is the vacuum permeability.

## 2. Results and discussion

### 2.1. Synthesis and X-ray structure

Model compounds **1** and **2** were both synthesized by means of Sonogashira cross coupling as depicted in Scheme 1. The spin labelled iodobiphenyl **5** is coupled to either the paramagnetic copper(meso-ethynyl-octaethylporphyrin) **6** or the diamagnetic nickel(meso-ethynyl-octaethylporphyrin) **7**. The final products **1** and **2** were both obtained as violet crystals after purification via column chromatography and subsequent crystallization.

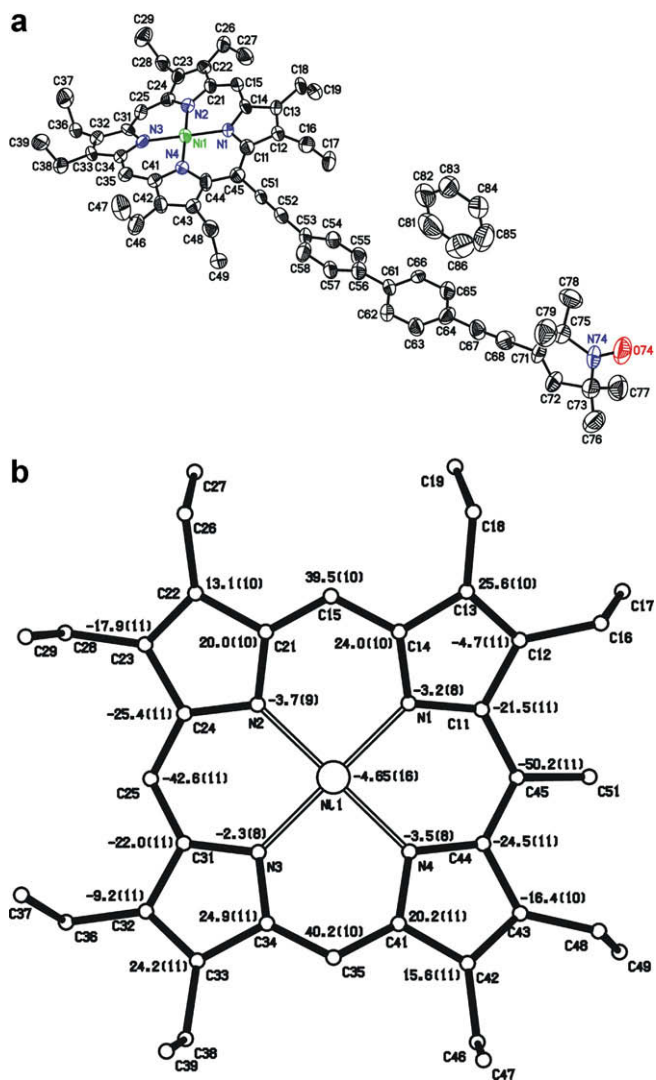


**Fig. 2.** (a) Molecular structure of **2**. Hydrogen atoms are omitted for clarity. (b) Formal diagram of the porphyrinato core of **2**. The displacements of each ring atom from the 24-atom core plane are illustrated. The structure is shown viewing perpendicular to the least-square plane calculated for the 24 core carbon and nitrogen atoms. Deviations are given in Å × 100 and calculated via  $D = 7.949(9)X - 6.460(10)Y - 10.707(13)Z + 0.286(7)$ , where  $X$ ,  $Y$ , and  $Z$  are the fractional coordinates.

The crystals obtained for **2** were suitable for X-ray diffraction and had a triclinic symmetry. A graphical representation of its

molecular structure is shown in Fig. 2a and selected bond lengths and angles are given in Tables 1 and 2. The porphyrin moiety exhibits significant deviations from planarity as commonly found for substituted metallo-porphyrins as for example the homo- and heterobimetallic ethene-linked bisporphyrins reported by Smith and coworkers [20]. Fig. 2b shows the ruffling of the porphyrinato core as formal diagram and Table 3 summarizes the angles between the least-squares planes of adjacent pyrrole rings. Despite the ruffled conformation, the distances between the nickel ion and the porphyrinato nitrogen atoms are all four in the range of 1.950(9) Å and 1.969(9) Å, which is in good agreement with the reported values of the planar parent compound nickel(octaethylporphyrin) [21]. The distances between the nickel ion and the nitrogen or the oxygen atom of the nitroxide group amount to 20.617(11) Å and 21.565(11) Å, respectively. Since the spin density in the N-O group is almost equally distributed between both centres, the mean distance of 21.087 Å will be used for the discussion. Crystals of **1** were not suitable for X-ray diffraction, however, due to their structural similarity the mean metal nitroxide distance gathered from **2** will be used instead.

## 2.2. CW EPR

To estimate the magnitude of the exchange coupling  $J$  in **1** cw X-band EPR spectra were recorded in toluene solution at room temperature. The resulting nitroxide spectrum is shown in Fig. 3a together with the spectrum of reference compound **3** (Fig. 3b). Both spectra are very similar as expected based on the structural similarity. However, a closer inspection of the nitroxide part reveals that the  $^1\text{H}$  hyperfine splitting pattern of the 12 methyl-protons is clearly visible for **3** but is unresolved for **1**. The reason is a larger line width, which is attributed to a larger exchange coupling. Thus, simulating the spectrum of **1** with the same set of parameters and values as used for **3** but increasing  $J$  from 0 to 3(1) MHz yields the simulation shown in Fig. 3a, which is in good agreement with the experiment. This value will be used in the following as a measure for the quality of the separation of  $J$  and  $D$  by the PELDOR experiment. An extraction of  $J$  and  $D$  from cw EPR spectra of **1** at 10 K (Fig. 3C) is not possible, due to the intrinsic large line width in frozen solutions and the small values for  $D$  and  $J$  [22].

## 2.3. PELDOR

The experimental PELDOR time traces of **1** and **3** are depicted in Fig. 4a. The traces have been acquired detecting the copper electron spin and pumping on the maximum of the nitroxide spectrum. A reference mixture of the unlabelled copper-porphyrin and the nitroxide spin-label, yielding only the typical monoexponential decay of mono radicals, was measured to ensure that the observed

**Table 1**  
Selected bond lengths for **2**.

	Distance, Å		Distance, Å		Distance, Å
Ni(1)–N(1)	1.958(7)	C(11)–C(12)	1.475(13)	C(34)–C(35)	1.392(14)
Ni(1)–N(2)	1.950(9)	C(12)–C(13)	1.366(14)	C(35)–C(41)	1.375(12)
Ni(1)–N(3)	1.964(7)	C(13)–C(14)	1.453(11)	C(41)–C(42)	1.473(14)
Ni(1)–N(4)	1.969(9)	C(14)–C(15)	1.433(14)	C(42)–C(43)	1.385(12)
N(1)–C(14)	1.364(12)	C(15)–C(21)	1.389(12)	C(43)–C(44)	1.466(14)
N(1)–C(11)	1.368(11)	C(21)–C(22)	1.485(13)	C(44)–C(45)	1.406(13)
N(2)–C(21)	1.373(12)	C(22)–C(23)	1.366(12)	C(45)–C(51)	1.445(12)
N(2)–C(24)	1.376(11)	C(23)–C(24)	1.474(15)	C(51)–C(52)	1.207(12)
N(3)–C(34)	1.356(12)	C(24)–C(25)	1.373(14)	C(67)–C(68)	1.219(12)
N(3)–C(31)	1.402(12)	C(25)–C(31)	1.357(14)	C(71)–C(72)	1.368(14)
N(4)–C(41)	1.372(12)	C(31)–C(32)	1.449(13)	N(74)–O(74)	1.271(10)
N(4)–C(44)	1.386(11)	C(32)–C(33)	1.360(14)	Ni(1)–N(74)	20.617(11)
C(11)–C(45)	1.452(14)	C(33)–C(34)	1.462(12)	Ni(1)–O(74)	21.565(11)

**Table 2**  
Selected bond angles for **2**.

	Angle, °		Angle, °
N(2)–Ni(1)–N(1)	91.4(4)	N(2)–C(21)–C(22)	111.8(8)
N(2)–Ni(1)–N(3)	89.0(4)	N(2)–C(24)–C(23)	111.9(9)
N(1)–Ni(1)–N(3)	178.8(4)	C(25)–C(24)–N(2)	124.8(10)
N(2)–Ni(1)–N(4)	179.3(4)	C(15)–C(21)–C(22)	122.2(10)
N(1)–Ni(1)–N(4)	89.0(3)	C(23)–C(22)–C(21)	105.6(9)
N(3)–Ni(1)–N(4)	90.6(3)	C(22)–C(23)–C(24)	106.1(9)
C(14)–N(1)–Ni(1)	126.2(6)	C(25)–C(24)–C(23)	123.2(9)
C(11)–N(1)–Ni(1)	129.9(7)	C(31)–C(25)–C(24)	123.8(9)
C(21)–N(2)–Ni(1)	127.0(6)	C(25)–C(31)–N(3)	124.6(9)
C(24)–N(2)–Ni(1)	128.4(7)	N(3)–C(31)–C(32)	111.0(10)
C(34)–N(3)–Ni(1)	127.6(6)	N(3)–C(34)–C(35)	124.4(8)
C(31)–N(3)–Ni(1)	127.4(7)	N(3)–C(34)–C(33)	111.1(9)
C(41)–N(4)–Ni(1)	125.1(6)	C(25)–C(31)–C(32)	124.3(9)
C(44)–N(4)–Ni(1)	128.9(7)	C(33)–C(32)–C(31)	105.9(9)
C(14)–N(1)–C(11)	103.8(7)	C(32)–C(33)–C(34)	107.1(9)
C(21)–N(2)–C(24)	104.6(8)	C(35)–C(34)–C(33)	124.3(10)
C(34)–N(3)–C(31)	104.9(8)	C(41)–C(35)–C(34)	123.5(10)
C(41)–N(4)–C(44)	106.0(8)	N(4)–C(41)–C(35)	127.0(10)
N(1)–C(11)–C(45)	123.3(9)	N(4)–C(41)–C(42)	110.7(8)
N(1)–C(11)–C(12)	112.3(9)	N(4)–C(44)–C(45)	124.2(10)
N(1)–C(14)–C(15)	125.8(8)	N(4)–C(44)–C(43)	110.9(8)
N(1)–C(14)–C(13)	112.8(9)	C(35)–C(41)–C(42)	122.3(10)
C(45)–C(11)–C(12)	124.4(8)	C(43)–C(42)–C(41)	106.4(9)
C(13)–C(12)–C(11)	104.9(8)	C(35)–C(41)–C(42)	122.3(10)
C(12)–C(13)–C(14)	106.1(9)	C(43)–C(42)–C(41)	106.4(9)
C(15)–C(14)–C(13)	121.2(10)	C(42)–C(43)–C(44)	105.9(8)
C(21)–C(15)–C(14)	121.8(10)	C(45)–C(44)–C(43)	124.8(9)
N(2)–C(21)–C(15)	126.0(10)	C(44)–C(45)–C(11)	121.3(9)

PELDOR effect is solely due to intramolecular spin–spin interaction and not to intermolecular interactions or instrumental artefacts. A PELDOR time trace of **2** cannot be recorded detecting the metal centre, since Ni(OEP) is diamagnetic.

The modulation depth of **1** and **3** are comparable, even though time traces of **1** are recorded with spectrally broader detection pulses of 16 ns instead of 32 ns. The shorter detection pulses proved to be necessary, since data recorded under the same conditions as for **3** did not bear visible oscillation and only a shallow modulation depth (data not shown). This is attributed to the fact that the pulse excitation bandwidth of 32 ns is not sufficiently large versus the spin–spin coupling leading to an incomplete detection of dipolar frequencies [23]. The frequency offset ( $\Delta\nu_{AB}$ ) between detection and pump frequency was set to 118 MHz. With smaller offsets, the excitation profiles of the pump and detection pulses overlap to such an extent that contributions from the nitroxide spin enter the refocused echo. At larger offsets it was not possible to achieve 16 ns detection pulses.

In addition, **1** and **3** show both modulations, but it is remarkable how fast the modulation is damped in **1**. Compound **3** displays three well resolved periods of modulation, whereas the modulation for **1** is barely visible. Commonly, a fast damping of a PELDOR modulation is attributed to a large conformational flexibility. However, the structural similarity of **1** and **3** renders an increased conformational flexibility as unlikely. In an earlier study, it was shown

that the relatively fast modulation damping in **3** compared to structurally similar bisnitroxides can be attributed to a small distribution in exchange couplings  $\Delta J = \pm 1$  MHz centred around  $J = 0$  MHz [12]. In principle the appearance of a small exchange coupling does not lead to drastic changes in the modulation damping, since it only shifts the frequencies of the dipolar tensor. Yet, a distribution in  $J$  has a similar effect as a distribution in  $r$ . Thus, the fast modulation damping in **1** may be attributed to a larger distribution in  $J$ . In order to prove that, we chose to simulate the time domain data to extract  $J$  and  $r$ . Available programs to invert the PELDOR time traces into the distance domain could not be used for this, since they neglect exchange contributions in the regularization kernels. It is also not possible to extract  $J$  and  $r$  from the Pake pattern after Fourier transformation of the time traces, as shown previously for a bisnitroxide system [24] since the singularities of the Pake pattern are not resolved (Fig. 4b).

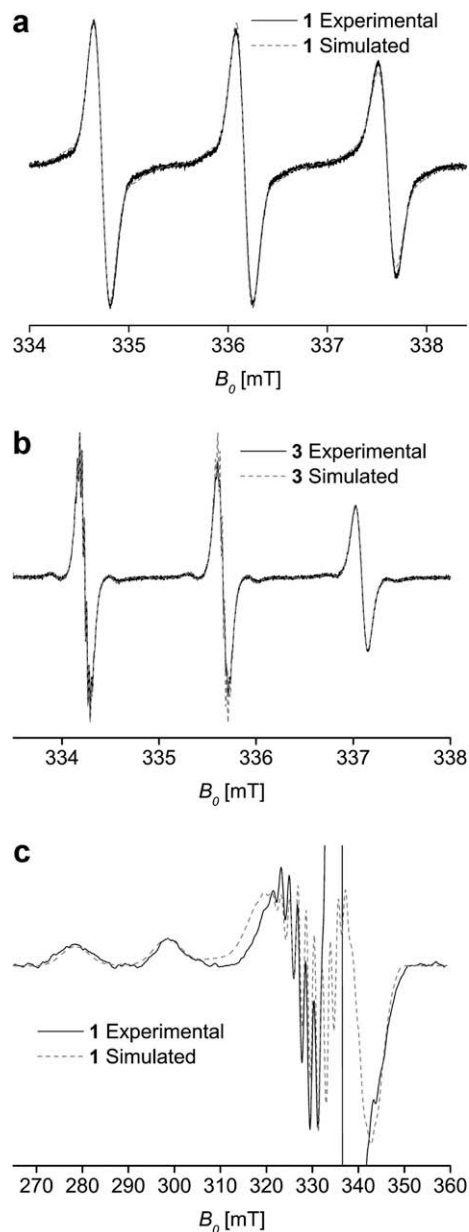
The simulations were performed in analogy to the procedure described for **3**. First, the excitation profiles in the nitroxide and Cu(OEP) molecular axis systems have been calculated using the values for the spectral parameters as gathered from the simulations of the cw EPR spectra.

Fig. 5 reveals that mainly copper-porphyrin moieties with the porphyrin plane parallel to the magnetic field are detected, whereas all orientation of the nitroxide moiety are inverted by the pump pulse. This orientation selection enters the PELDOR simulations via the form factor, which describes the excitation probability with respect to the dipolar angle  $\theta$ . The form factor has been calculated for an ensemble of conformers generated from a geometric model based on the crystal structure of **2**. The model (Fig. 5d) is essentially the same as used for **3** but taking into account that the mean metal/nitroxide distance equals 21 Å, instead of 20.7 Å and that the free rotation of the nitroxide group around the linker bond is on a cone of 39°, instead of 31.4°. A single bending motion of 15° centred at the mid-point of the biphenyl bridge enters both models. The resulting distribution function of dipolar angles shown in Fig. 6 displays a strong deviation from a  $\sin(\theta)$  distribution, which describes the form factor of a system without angular correlation. Distance vectors parallel to the magnetic field become more probable, whereas distance vectors perpendicular to the magnetic field are deselected, which can be rationalized by the deselection of Cu(OEP) moieties with the porphyrin ring plane perpendicular to the magnetic field. Thus, the most prominent feature of the dipolar Pake pattern is deselected, the theoretical dipolar spectrum for this distribution of dipolar angles is shown in Fig. 6b.

Simulating with this form factor the PELDOR time trace reveals that the data can not be satisfactorily reproduced (data not shown). Taking a singular exchange coupling constant into account does also not lead to better simulations (Fig. 7), but including a distribution  $\Delta J = \pm 5(1)$  MHz centred around  $+4(1)$  MHz (antiferromagnetic) achieves very good agreement between experiment and simulation (see Fig. 7). A negative  $J$  (ferromagnetic) leads to completely different results (data not shown). And indeed, the antiferromagnetic exchange coupling of 4(1) MHz is in agreement with the value of 3(1) MHz determined from the room temperature cw EPR spec-

**Table 3**  
Angles (°) between the pyrrole best planes of compound **2**. X, Y, and Z are in triclinic fractional coordinates.

	Plane 2	Plane 3	Plane 4
Plane 1	15.1(6)	26.1(6)	20.2(6)
Plane 2		20.0(6)	24.6(6)
Plane 3			15.6(6)
Plane 1, Pyrrole ring 1. N(1), C(11)–C(14) – 6.47(6)X + 5.32(7)Y + 13.34(7)Z = 2.17(5)			
Plane 2, Pyrrole ring 2. N(2), C(21)–C(24) – 5.79(6)X + 8.22(5)Y + 12.25(7)Z = 0.51(5)			
Plane 3, Pyrrole ring 3. N(3), C(31)–C(34) 8.96(4)X – 7.41(5)Y – 7.52(9)Z = 1.41(5)			
Plane 4, Pyrrole ring 4. N(4), C(41)–C(44) 9.74(5)X – 4.45(7)Y – 8.66(8)Z = – 0.11(2)			



**Fig. 3.** CW X-band EPR spectra of the nitroxide part of (a) model compound **1** and (b) reference **3**, both at room temperature. (c) Spectrum of the copper centre of **1** acquired at 10 K and with a microwave power of 100 mW saturating the nitroxide centre. The solid black lines are the experimental spectra, the broken grey lines are the simulations.

trum. Thus, **1** possesses a larger exchange coupling than **3**, as anticipated from the conjugated bridge and the exchange coupling is antiferromagnetic as usually found for copper-nitroxide systems of such geometries [25]. The reason for the distribution in  $J$  is the ensemble of conformers. The different conformers possess different orbital overlaps and thus different magnitudes for the through bond exchange coupling constant. Thus, the increased modulation damping in the PELDOR time trace of **1** compared to **3**, can be rationalized by the larger  $J$ , +4 MHz compared to 0 MHz, and larger  $\Delta J$ ,  $\pm 5$  MHz compared to  $\pm 1$  MHz, respectively.

#### 2.4. Conclusion

We have shown on a copper/nitroxide model system that PELDOR in combination with simulations allows for separating the

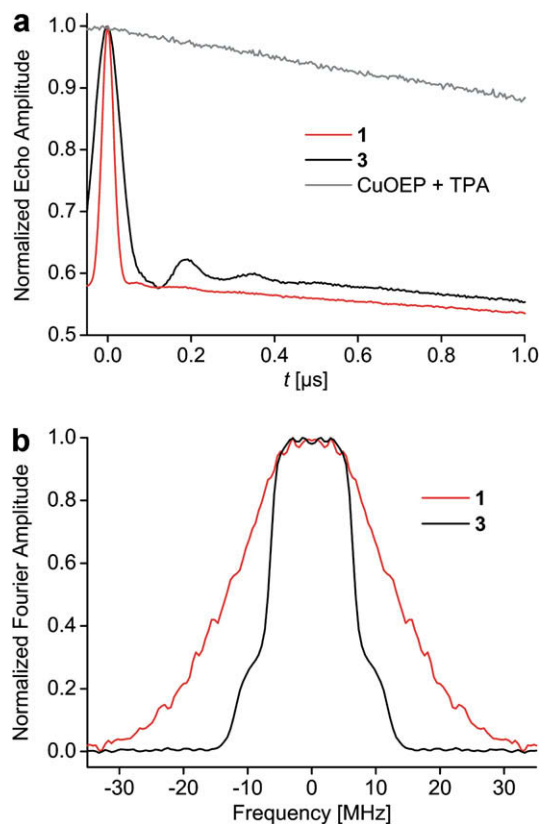


**Fig. 4.** (a) PELDOR time domain data of **1**, **3** and a reference mixture of Cu(OEP) and TPA. (b) Dipolar spectra obtained by Fourier transformation of the time traces above.

dipolar through space coupling from the through bond exchange coupling, even if the singularities of the Pake pattern are not resolved. This enables one to evaluate structural models on the basis of PELDOR measurements between a copper ion and a nitroxide even in the presence of an exchange coupling. Furthermore, not only the magnitude, but also the sign of the exchange coupling and the distribution in  $J$  can be gathered. It is, however, mandatory, that the spin–spin coupling tensor is smaller than the excitation band width of the pulses, which limits the method to small exchange couplings and rather long distances. Thus, PELDOR complements nicely other methods capable to measure  $J$ : Large exchange coupling constants can be determined with their sign via temperature dependent Squid measurements [26] or via temperature dependent measurements of the intensity of the half-field EPR signal [27]. Exchange coupling constants on the order of the hyperfine coupling can be obtained via simulations of the isotropic main field EPR signal but without sign [28] and small exchange coupling constants are accessible from PELDOR spectra.

### 3. Experimental

#### 3.1. Synthesis

All reactions were performed with exclusion of air under argon employing standard Schlenk techniques. Reagent-grade solvents and chemicals were used without further purification, except where stated otherwise. Dry solvents were purchased from Fluka or ACROS and thoroughly degassed prior to use. Triethylamine was freshly distilled from  $\text{CaH}_2$ .  $D_{14}$ -*o*-terphenyl was purchased from Cambridge Isotope Laboratories and used without further purification. Octaethylporphyrin ( $\text{H}_2(\text{OEP})$ ) and copper(II)-octaethylporphyrin

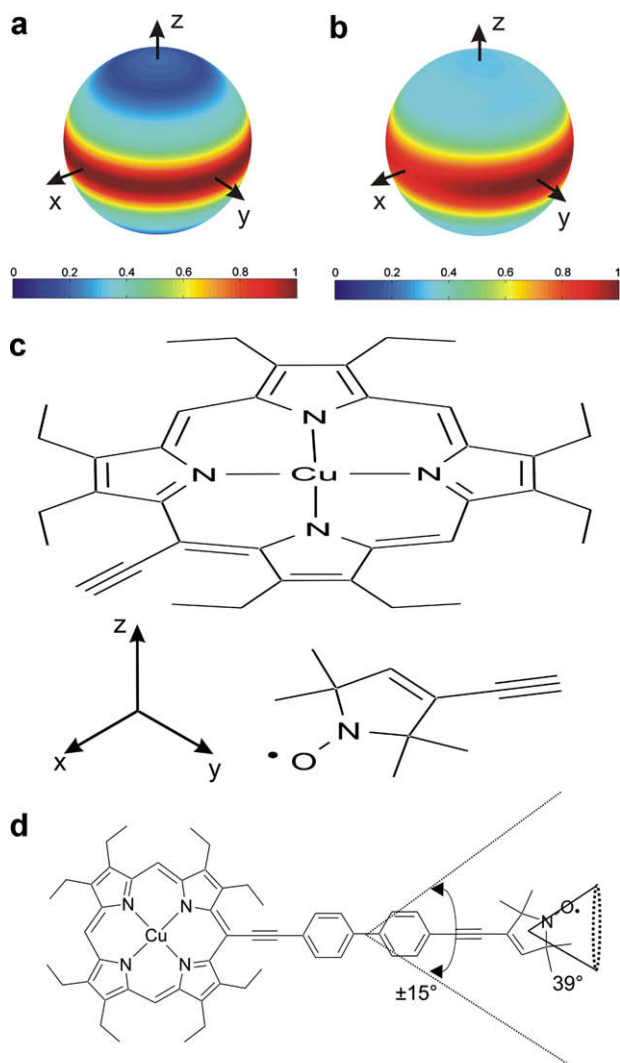


**Fig. 5.** Excitation profiles of (a) the detection pulses on the Cu(OEP) and (b) the pump pulse on the nitroxide. The molecular axis systems are defined in (c). The geometric model is depicted in (d).

(Cu(OEP)) were purchased from Aldrich, thin layer chromatography plates SiO<sub>2</sub> 60 F<sub>254</sub> and Al<sub>2</sub>O<sub>3</sub> 60 F<sub>254</sub> neutral were bought from Merck, SiO<sub>2</sub> 60 (70–230 mesh) and Al<sub>2</sub>O<sub>3</sub> MP Alumina N – Super I were used from Aldrich or MP Biomedicals, respectively. 1-Oxyl-2,2,5,5-tetramethylpyrrolin-3-acetylene (TPA) **4** [29] and 3-(4'-Iodo-biphenyl-4-ylethynyl)-2,2,5,5-tetramethylpyrrolin-1-oxyl **5** [10] were prepared by procedures described earlier. Cu(meso-ethynyl-OEP) **6** and Ni(meso-ethynyl-OEP) **7** were prepared according to references [16,30] and used as obtained, due to the products susceptibility to spontaneous oxidative dimerisation [31].

Analytic relied on elemental analysis and mass spectrometry such as EI, ESI, and MALDI. EI mass spectra were recorded on a CH7A spectrometer from MAT, ESI mass spectra on a LCQ Classic spectrometer from Thermo Electron and MALDI mass spectra on a Voyager DE-Pro or STR spectrometer, both from Applied Biosystems. Proton NMR spectra of diamagnetic molecules were acquired at 250 MHz on a Bruker AM-250 spectrometer and calibrated using residual non-deuterated solvents as internal standard ( $\delta$  CHCl<sub>3</sub> = 7.240). Elementary analysis was performed on a Foss-Heraeus CHN-O-Rapid and UV-Vis spectra were recorded on an Agilent 8453 Spectrophotometer.

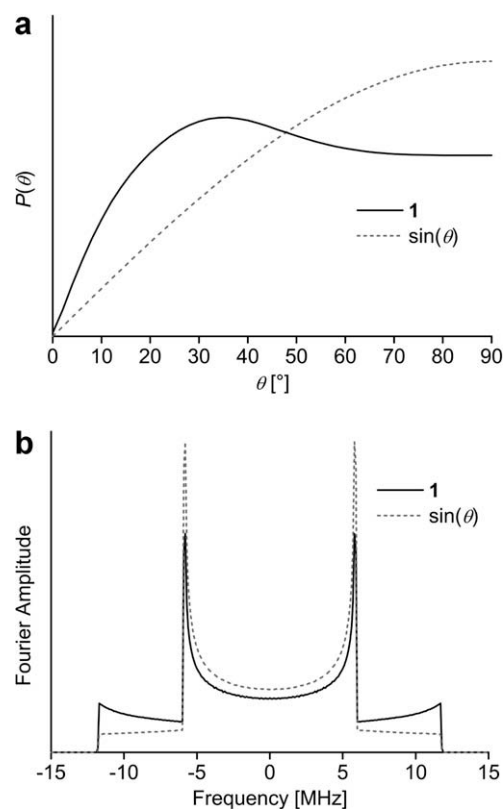


**Fig. 6.** (a)  $P(\theta)$  of **1**. A  $\sin(\theta)$  distribution for random orientations is shown for comparison. (b) Dipolar spectra calculated from  $P(\theta)$  assuming a distance of 2.1 nm and a  $J$  of 0 MHz.

### 3.1.1. Synthesis of (3-(4'-copper(II)-2,3,7,8,12,13,17,18-octaethylporphyrin-5-ylethynyl-biphenyl-4-ylethynyl)-2,2,5,5-tetramethyl-pyrrolin-1-oxyl) (**1**)

3-(4'-Iodo-biphenyl-4-ylethynyl)-2,2,5,5-tetramethyl-pyrrolin-1-oxyl **5** (80 mg, 0.18 mmol) and PdCl<sub>2</sub>(PPh<sub>3</sub>)<sub>2</sub> (19 mg, 0.027 mmol) were dissolved in NEt<sub>3</sub> (12 mL) and DMF (5 mL) by slightly warming the mixture. CuI (19 mg, 0.100 mmol) was added, followed by a solution of Cu(meso-ethynyl-OEP) **6** (112 mg, 0.18 mmol) and PPh<sub>3</sub> (18 mg, 0.06 mmol) in NEt<sub>3</sub> (8 mL) and DMF (3 mL). The mixture was stirred for 16 h at 60 °C. The solvents were removed in vacuo, the residue dissolved in dichloromethane and washed three times with water. The organic phase was dried with sodium sulphate, and the solvent was removed in vacuo.

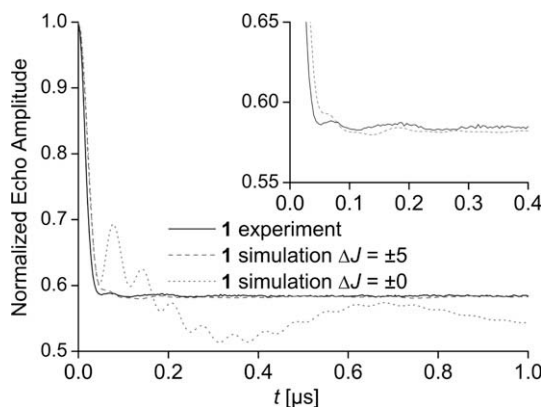


**Fig. 7.** Background corrected PELDOR data of **1** and its simulations based on an exchange coupling of  $J = +4$  MHz and a  $\Delta J$  of  $\pm 5$  MHz or  $\pm 0$  MHz.

Chromatography (4 × 20 cm, Al<sub>2</sub>O<sub>3</sub>, 4% H<sub>2</sub>O, CHCl<sub>3</sub>/hexane 1:1 to 2:1) yielded a slow moving red-brown main band after three zones of green, pink and light green colour all three of weak intensity. The red-brown product fraction was collected and stripped from solvent. The residue was further purified by repeated (2 ×) chromatography (3 × 20 cm, Al<sub>2</sub>O<sub>3</sub>, 4% H<sub>2</sub>O, CH<sub>2</sub>Cl<sub>2</sub>) to remove a green by-product. The desired product was then recrystallised two times from chloroform/methanol and finally from benzene layered with petroleum ether. Compound **1** was obtained as thin violet leaflets and needles. Yield: 65 mg (0.07 mmol, 39%). Anal. Calc. for C<sub>60</sub>H<sub>64</sub>N<sub>5</sub>OCu: C, 77.10; H, 6.90; N, 7.49. Found: C, 77.37; H, 6.89; N, 7.52%. UV-Vis (benzene) λ<sub>max</sub> (log ε): 427 nm (5.389), 554 (4.274), 594 (4.273). MALDI-TOF-MS *m/z* Calc. for C<sub>60</sub>H<sub>64</sub>N<sub>5</sub>OCu: 934.746; found: 936.6 ((M + 2 × H)<sup>+</sup>, 100%), 919.6 ((M + 2 × H - CH<sub>3</sub>)<sup>+</sup>, 32%), 875.7 ((M + 2 × H - 4 × CH<sub>3</sub>)<sup>+</sup>, 28%).

### 3.1.2. Synthesis of (3-(4'-nickel(II)-2,3,7,8,12,13,17,18-octaethylporphyrin-5-ylethynyl-biphenyl-4-ylethynyl)-2,2,5,5-tetramethyl-pyrrolin-1-oxyl) (**2**)

To a suspension of **5** (27 mg, 0.06 mmol) and PdCl<sub>2</sub>(PPh<sub>3</sub>)<sub>2</sub> in 5 mL NEt<sub>3</sub> a solution of Ni(meso-ethynyl-OEP) **7** (37 mg, 0.06 mmol) in 10 mL NEt<sub>3</sub> was added at room temperature via syringe. The resulting red solution was heated to gentle reflux for 3.5 h and stirred for additional 16 h at ambient temperature. From the red-brown solution a yellowish precipitate was formed. The solvent was removed in vacuo, the residue dissolved in 2–4 mL dichloromethane/hexane (1:1) and subjected to column chromatography (3 × 25 cm, Al<sub>2</sub>O<sub>3</sub>, 3% H<sub>2</sub>O). A dark green band was eluted first, followed by a broad red band of the main product. The main fraction was brought to dryness and the residue washed with a small amount of hexane. Recrystallisation from chloroform/methanol yielded 32 mg (0.03 mmol, 57%) of **2** as thin, lustrous violet platelets and needles. Suitable crystals for x-ray diffraction were obtained from benzene solution layered with petroleum ether. Anal. Calc. for C<sub>60</sub>H<sub>64</sub>N<sub>5</sub>ONi: C, 77.50; H, 6.94; N, 7.53. Found: C, 77.30; H, 6.98; N, 7.48%. UV-Vis (benzene) λ<sub>max</sub> (log ε): 432 nm (5.326), 557 (4.227), 592 (4.260). MALDI-TOF-MS (matrix, DHB) *m/z* Calc. for C<sub>60</sub>H<sub>64</sub>N<sub>5</sub>NiO: 929.901; Found: 930.3 (M<sup>+</sup>, 100%), 914.3 ((M - CH<sub>3</sub>)<sup>+</sup>, 12%), 899.2 ((M - 2 × CH<sub>3</sub>)<sup>+</sup>, 12%).

### 3.2. X-ray crystallography

Data of **2** · C<sub>6</sub>H<sub>6</sub> were collected at 173 K on a STOE IPDS II two-circle diffractometer using Mo Kα radiation. The structure was solved using direct methods and refined on *F*<sup>2</sup> values using the full-matrix least-squares method. Programs used include X-AREA (STOE & CIE GmbH, Darmstadt, Germany, 2001), SHELXS-97 (G.M. Sheldrick, University of Göttingen, Germany, 1997), SHELXTL-Plus (Release 4.1, Siemens Analytical X-ray Instruments Inc., Madison, Wisconsin, USA). The SHELXL-97, PLATON [33] and MERCURY [34] software has been used to prepare material for publication. Graphical representations of the crystal structure were produced using the WinGX software [35].

Crystal data: Empirical formula: C<sub>66</sub>H<sub>70</sub>N<sub>5</sub>NiO, formula weight: 1007.98, temperature: 173(2) K, wavelength: 0.71073 Å, crystal system: triclinic, space group: *P*1̄, unit cell dimensions: *a* = 12.639(4) Å, *b* = 13.134(4) Å, *c* = 82.56(3) Å, *α* = 73.80(3)°, *β* = 87.32(3)°, *γ* = 87.32(3)°, volume: 2772.3(15) Å<sup>3</sup>, *Z* = 2, *D*<sub>calc</sub>: 1.207 Mg/m<sup>3</sup>, absorption coefficient: 0.397 mm<sup>-1</sup>, *F*(000): 1074, crystal size: 0.42 × 0.14 × 0.03 mm<sup>3</sup>, *θ*-range for data collection: 3.61°–25.12°, *hkl* index ranges: 14/14, 15/15, 20/20, reflections collected: 16491, independent reflections: 9042 [*R*<sub>int</sub> = 0.1828], completeness to *θ* = 25.12°: 91.3%, absorption correction: semi-empirical from equivalents, maximum and minimum transmission: 0.9882 and 0.8510, refinement method: full-matrix least-squares on *F*<sup>2</sup>, data/restraints/parameters: 9042/0/658, goodness-of-fit on *F*<sup>2</sup>: 0.841, final

*R* indices [*I* > 2σ(*I*): *R*<sub>1</sub> = 0.0869, *wR*<sub>2</sub> = 0.1232, *R* indices (all data): *R*<sub>1</sub> = 0.2730, *wR*<sub>2</sub> = 0.1862, largest difference in peak/hole: 0.404/0.583 e Å<sup>-3</sup>. Crystallographic data for the structural analysis has been deposited with the Cambridge Crystallographic Data Centre, CCDC No. 614808 for compound **2** · C<sub>6</sub>H<sub>6</sub>.

### 3.3. EPR measurements

Samples of **1** and **2** were prepared as a *d*<sub>8</sub>-toluene and *d*<sub>14</sub>-*o*-terphenyl (both 200 μM, 80 μL) solutions. Five equivalents of 1-methylimidazole were added to samples of **1**, to prevent aggregation. The *d*<sub>8</sub>-toluene sample was degassed by several freeze-pump cycles and frozen in liquid nitrogen prior to sealing the sample tube.

The cw X-band EPR spectra were acquired on a Bruker ELEXSYS E500 cw X-band EPR spectrometer equipped with a standard rectangular Bruker EPR cavity (ER4102T) equipped with an Oxford helium cryostat (ESR900). The microwave frequency was measured by use of a Systron Donner (6054D) frequency counter. The magnetic field was measured with a Bruker gaussmeter (ER035M). All room temperature spectra were recorded with a sampling time of 40 ms, a microwave power of 1 mW and a modulation amplitude of 1 μT at a modulation frequency of 100 kHz. Low temperature spectra were recorded at 10 K, with a microwave power of 100 mW and a modulation amplitude of 0.5 mT at a modulation frequency of 100 kHz. All cw X-band spectra simulations were performed with EasySpin [36]. The room temperature nitroxide spectra were simulated using *g*<sub>xx</sub> = 2.0095, *g*<sub>yy</sub> = 2.0071, *g*<sub>zz</sub> = 2.0036 and *A*<sub>xx</sub> = 0.4 mT, *A*<sub>yy</sub> = 0.3 mT, *A*<sub>zz</sub> = 3.1 mT for the <sup>14</sup>N hyperfine coupling. The isotropic <sup>1</sup>H hyperfine coupling of the 12 equiv. methyl-protons was set to 0.65 MHz and to 1.3 MHz for the vinylic proton. An isotropic <sup>13</sup>C hyperfine coupling constant of 16.5 MHz was assumed for the α- and methyl-carbons all with natural abundance. The residual Lorentzian line width is 0.3 MHz and an axial diffusion tensor with *D*<sub>xy</sub> = 1 GHz and *D*<sub>zz</sub> = 100 GHz was assumed. All values are in good agreement with literature values [27,37]. The low temperature spectrum of the copper(II) centre has been simulated using *g*<sub>xx</sub> = *g*<sub>yy</sub> = 2.047, *g*<sub>zz</sub> = 2.17 and a *g*-strain of *g*<sub>xx</sub> = *g*<sub>yy</sub> = 0.005, *g*<sub>zz</sub> = 0.015 and *A*<sub>xx</sub> = *A*<sub>yy</sub> = 3 mT, *A*<sub>zz</sub> = 21 mT for the Cu hyperfine coupling. The <sup>14</sup>N hyperfine coupling of the four porphyrin nitrogen atoms was assumed to be isotropic and set to 1.7 mT. The residual line width was 1.3 mT.

All PELDOR spectra were recorded on a Bruker ELEXSYS E580 pulsed X-band EPR spectrometer with a standard flex line probe head housing a dielectric ring resonator (MD5 W1) equipped with a continuous flow helium cryostat (CF935) and temperature control system (ITC 502), both from Oxford instruments. The second microwave frequency was coupled into the microwave bridge by a commercially available setup (E580-400U) from Bruker. All pulses were amplified via a pulsed travelling wave tube (TWT) amplifier (117X) from Applied Systems Engineering. The resonator was over-coupled to a quality factor *Q* of about 50. PELDOR experiments were performed with the pulse sequence π/2(*v*<sub>A</sub>)–τ<sub>1</sub>–π(*v*<sub>A</sub>)–(τ<sub>1</sub> + *t*)–π(*v*<sub>B</sub>)–(τ<sub>2</sub> – *t*)–π(*v*<sub>A</sub>)–τ<sub>2</sub>–echo. The detection pulses (*v*<sub>A</sub>) were set to 16 ns for both π and π/2-pulses and applied at a frequency 118 MHz higher than the resonance frequency of the resonator. The pulse amplitudes were chosen to optimize the refocused echo. The π/2-pulse was phase-cycled to eliminate receiver offsets. The pump pulse (*v*<sub>B</sub>) with a length of 12 ns was set at the resonance frequency of the resonator. The field was adjusted such that the pump pulse is applied to the maximum of the nitroxide spectrum, where it selects the central *m*<sub>l</sub> = 0 transition of *A*<sub>zz</sub> together with the *m*<sub>l</sub> = 0, ±1 transitions of *A*<sub>xx</sub> and *A*<sub>yy</sub>. The pulse amplitude was optimized to maximize the inversion of a Hahn-echo at the pump frequency. All PELDOR spectra were recorded at 20 K with an experiment repetition time of 3 ms, a video amplifier bandwidth of 25 MHz and an amplifier gain of 63 dB. τ<sub>1</sub> was set

to 136 ns and  $\tau_2$  to 1200 ns. Usually 300 scans were accumulated with 294 data points and time increments  $\Delta t$  of 4 ns giving an approximate measurement time of 18 h necessary to obtain a signal-to-noise ratio >200:1. Proton modulation was suppressed by addition of eight spectra of variable  $\tau_1$  with a  $\Delta\tau_1$  of 8 ns [38]. For comparison with simulations the time traces were divided by a monoexponential decay and normalized to the point  $t = 0$ .

### 3.4. PELDOR simulations

Commonly PELDOR data are analyzed by using data inversion methods like Tikhonov regularization [39]. However, up to now all these methods are based on the assumption of negligible angular correlations and exchange coupling contributions, which can lead to erroneous results for systems like **1** and **3**. We have, therefore, chosen to simulate the experimental PELDOR time traces of **1** with a home-written Matlab® program, in analogy to the procedure as described for **3** in references [16,40].

### Acknowledgements

We thank Dr. Ute Bahr, Goethe-University, for recording mass spectra. This work has been supported by the Deutsche Forschungsgemeinschaft (SFB 579 “RNA-ligand interactions”) and the Center for Biomolecular Magnetic Resonance (BMRZ) Frankfurt.

### References

- [1] M. Ruben, J. Rojo, F.J. Romero-Salguero, L.H. Uppadine, J.-M. Lehn, *Angew. Chem., Int. Ed.* 43 (2004) 3644.
- [2] (a) A. Messerschmidt, R. Huber, T. Poulos, K. Wieghardt (Eds.), *Handbook of Metalloproteins*, vols. 1–2, John Wiley & Sons, Ltd., Chichester, 2001; (b) W.F. DeGrado, C.M. Summa, V. Pavone, F. Nistri, A. Lombardi, *Ann. Rev. Biochem.* 68 (1999) 779.
- [3] (a) F. Eckstein, D.M. Lilley, *Nucleic acids and molecular biology*, Catalytic RNA, vol. 10, Springer, Berlin, 1995; (b) R.F. Gesteland, T.R. Cech, J.F. Atkins, *The RNA World*, third ed., Cold Spring Harbor, New York, 2006.
- [4] (a) M. Ubbink, J.A.R. Worrall, G.W. Canters, E.J.J. Groenen, M. Huber, *Ann. Rev. Biophys. Biomol. Struct.* 31 (2002) 393; (b) C. Calle, A. Srekanth, M.V. Fedin, J. Forrer, I. Garcia-Rubio, I.A. Gromov, D. Hinderberger, B. Kasumaj, P. Léger, B. Mancosu, G. Mitrikas, M.G. Santangelo, S. Stoll, A. Schweiger, R. Tschaggelar, J. Harmer, *Helv. Chim. Acta* 89 (2006) 2495; (c) N. Kisseleva, S. Kraut, A. Jäschke, O. Schiemann, *HFSP J.* 1 (2007) 127; (d) N. Kisseleva, A. Khvorova, E. Westhof, O. Schiemann, *RNA* 11 (2005) 1.
- [5] (a) G. Jeschke, Y. Polyhach, *Phys. Chem. Chem. Phys.* 9 (2007) 1895; (b) O. Schiemann, T.F. Prisner, *Quart. Rev. Biophys.* 40 (2007) 1.
- [6] (a) A.D. Milov, K.M. Salikhov, M.D. Shirov, *Fiz. Tverd. Tela* 23 (1981) 975; (b) R.E. Martin, M. Pannier, F. Diederich, V. Gramlich, M. Hubrich, H.W. Spiess, *Angew. Chem., Int. Ed.* 37 (1998) 2833.
- [7] (a) M. Bennati, A. Weber, J. Antonic, D.L. Perlstein, J. Robblee, J. Stubbe, *J. Am. Chem. Soc.* 125 (2003) 14988; (b) G. Jeschke, *Macromol. Rapid Commun.* 23 (2002) 227; (c) O. Schiemann, N. Piton, Y. Mu, G. Stock, J.W. Engels, T.F. Prisner, *J. Am. Chem. Soc.* 126 (2004) 5722; (d) S.-Y. Park, P.P. Borbat, G. Gonzalez-Bonet, J. Bhatnagar, A.M. Pollard, J.H. Freed, A.M. Bilwes, B.R. Crane, *Nat. Struct. Mol. Biol.* 13 (2006) 400.
- [8] A. Godt, M. Schulte, H. Zimmermann, G. Jeschke, *Angew. Chem., Int. Ed.* 45 (2006) 7560.
- [9] (a) V.P. Denysenkov, T.F. Prisner, J. Stubbe, M. Bennati, *Proc. Natl. Acad. Sci. USA* 103 (2006) 13386; (b) Y. Polyhach, A. Godt, C. Bauer, G. Jeschke, *J. Magn. Reson.* 185 (2007) 118; (c) A. Savitsky, A.A. Dubinskii, M. Flores, W. Lubitz, K. Möbius, *J. Phys. Chem. B* 111 (2007) 6245.
- [10] B.E. Bode, D. Margraf, J. Plackmeyer, G. Dürner, T.F. Prisner, O. Schiemann, *J. Am. Chem. Soc.* 129 (2007) 6736.
- [11] E. Narr, A. Godt, G. Jeschke, *Angew. Chem., Int. Ed.* 41 (2002) 3907.
- [12] (a) I.M.C.v. Amsterdam, M. Ubbink, G.W. Canters, M. Huber, *Angew. Chem., Int. Ed.* 42 (2003) 62; (b) C.W.M. Kay, H.E. Mkami, R. Cammack, R.W. Evans, *J. Am. Chem. Soc.* 129 (2007) 4868; (c) Z. Yang, J. Becker, S. Saxena, *J. Magn. Reson.* 188 (2007) 337.
- [13] A.M. Raitsimring, C. Gunanathan, A. Potapov, I. Efremenko, J.M.L. Martin, D. Milstein, D. Goldfarb, *J. Am. Chem. Soc.* 129 (2007) 14138.
- [14] C. Elsässer, M. Brecht, R. Bittl, *J. Am. Chem. Soc.* 124 (2002) 12606.
- [15] A.V. Astashkin, J. Seravalli, S.O. Mansoorabadi, G.H. Reed, S.W. Ragsdale, *J. Am. Chem. Soc.* 128 (2006) 3888.
- [16] B.E. Bode, J. Plackmeyer, T.F. Prisner, O. Schiemann, *J. Phys. Chem. A* 112 (2008) 5064.
- [17] S.O. Mansoorabadi, G.H. Reed, in: J. Telsler (Ed.), *Paramagnetic Resonance of Metallobiomolecules*, American Chemical Society, Washington, 2003, p. 82.
- [18] W.B. Mims, in: S. Geschwind (Ed.), *Electron Paramagnetic Resonance*, Plenum, New York, 1972, p. 263.
- [19] (a) R.G. Larsen, D.J. Singel, *J. Chem. Phys.* 98 (1993) 5134; (b) A.D. Milov, A.G. Maryasov, Y.D. Tsvetkov, *Appl. Magn. Reson.* 15 (1998) 107.
- [20] (a) M.O. Senge, M.G.H. Vicente, K.R. Gerzsevske, T.P. Forsyth, K.M. Smith, *Inorg. Chem.* 33 (1994) 5625; (b) T.E. Clement, D.J. Nurco, K.M. Smith, *Inorg. Chem.* 37 (1998) 1150.
- [21] D.L. Cullen, E.F. Meyer Jr., *J. Am. Chem. Soc.* 96 (1974) 2095.
- [22] Low temperature cw X-band EPR spectra of **1** and **3** showed strong half-field signals at  $g = 4$  indicative of close spin–spin contacts. These signals disappeared completely upon adding 1-methylimidazole pointing to intermolecular stacking of these compounds as the origin for this strong spin–spin coupling which can be disrupted by coordination of 1-methylimidazole to copper(II) as known from the literature.
- [23] (a) A.G. Maryasov, Yu.D. Tsvetkov, *Appl. Magn. Reson.* 18 (2000) 583; (b) A.D. Milov, B.D. Naumov, Y.D. Tsvetkov, *Appl. Magn. Reson.* 26 (2004) 587.
- [24] A. Weber, O. Schiemann, B. Bode, T.F. Prisner, *J. Magn. Reson.* 157 (2002) 277.
- [25] (a) O. Kahn, *Molecular Magnetism*, VCH, New York, 1993; (b) S.S. Eaton, K.M. More, B.M. Sawant, P.M. Boymel, G.R. Eaton, *J. Magn. Reson.* 50 (1983) 435.
- [26] (a) C. Elschenbroich, O. Schiemann, O. Burghaus, K. Harms, J. Pebler, *Organometallics* 18 (1999) 3273; (b) C. Elschenbroich, M. Wolf, O. Schiemann, K. Harms, O. Burghaus, J. Pebler, *Organometallics* 21 (2002) 5810; (c) C. Elschenbroich, J. Plackmeyer, K. Harms, O. Burghaus, J. Pebler, *Organometallics* 22 (2003) 3369; (d) C. Elschenbroich, J. Plackmeyer, M. Nowotny, K. Harms, J. Pebler, O. Burghaus, *Inorg. Chem.* 44 (2005) 955; (e) C. Elschenbroich, O. Schiemann, O. Burghaus, K. Harms, *Chem. Commun.* (2005) 2149.
- [27] J. Fritscher, M. Beyer, O. Schiemann, *Chem. Phys. Lett.* 364 (2002) 393.
- [28] C. Elschenbroich, O. Schiemann, O. Burghaus, K. Harms, *J. Am. Chem. Soc.* 119 (1997) 7452.
- [29] (a) T. Kálai, M. Balog, J. Jekő, K. Hideg, *Synthesis* (1999) 973; (b) O. Schiemann, N. Piton, J. Plackmeyer, B.E. Bode, T.F. Prisner, J.W. Engels, *Nat. Protoc.* 2 (2007) 904.
- [30] N. Hayashi, M. Murayama, K. Mori, A. Matsuda, E. Chikamatsu, K. Tani, K. Miyabayashi, M. Miyake, H. Higuchi, *Tetrahedron* 60 (2004) 6363.
- [31] (a) D.P. Arnold, D.A. James, *J. Org. Chem.* 62 (1997) 3460; (b) D.P. Arnold, R.D. Hartnell, *Tetrahedron* 57 (2001) 1335.
- [32] G.M. Sheldrick, *Acta Crystallogr. A* 46 (1990) 467.
- [33] A.L. Spek, *J. Appl. Crystallogr.* 36 (2003) 7.
- [34] (a) I.J. Bruno, J.C. Cole, P.R. Edgington, M.K. Kessler, C.F. Macrae, P. McCabe, J. Pearson, R. Taylor, *Acta Crystallogr. B* 58 (2002) 389; (b) C.F. Macrae, P.R. Edgington, P. McCabe, E. Pidcock, G.P. Shields, R. Taylor, M. Towler, J. van de Streek, *J. Appl. Crystallogr.* 39 (2006) 453.
- [35] L.J. Farrugia, *J. Appl. Crystallogr.* 32 (1999) 837.
- [36] S. Stoll, A. Schweiger, *J. Magn. Reson.* 178 (2006) 42.
- [37] (a) R.W. Kreilick, *J. Chem. Phys.* 46 (1967) 4260; (b) G.F. Hatch, R.W. Kreilick, *J. Chem. Phys.* 57 (1972) 3696.
- [38] G. Jeschke, G. Panek, A. Godt, A. Bender, H. Paulsen, *Appl. Magn. Reson.* 26 (2004) 223.
- [39] (a) G. Jeschke, V. Chechik, P. Ionita, A. Godt, H. Zimmermann, J. Banham, C.R. Timmel, D. Hilger, H. Jung, *Appl. Magn. Reson.* 30 (2006) 4733; (b) M.K. Bowman, A.G. Maryasov, N. Kim, V.J. DeRose, *Appl. Magn. Reson.* 26 (2004) 23; (c) Y.-W. Chiang, P.P. Borbat, J.H. Freed, *J. Magn. Reson.* 172 (2005) 279.
- [40] D. Margraf, B.E. Bode, A. Marko, O. Schiemann, T.F. Prisner, *Mol. Phys.* 105 (2007) 2153.